Stem Cell Reports, Volume *15*

Supplemental Information

Identification of Qk as a Glial Precursor Cell Marker that Governs the Fate Specification of Neural Stem Cells to a Glial Cell Lineage

Akihide Takeuchi, Yuji Takahashi, Kei Iida, Motoyasu Hosokawa, Koichiro Irie, Mikako Ito, J.B. Brown, Kinji Ohno, Kinichi Nakashima, and Masatoshi Hagiwara

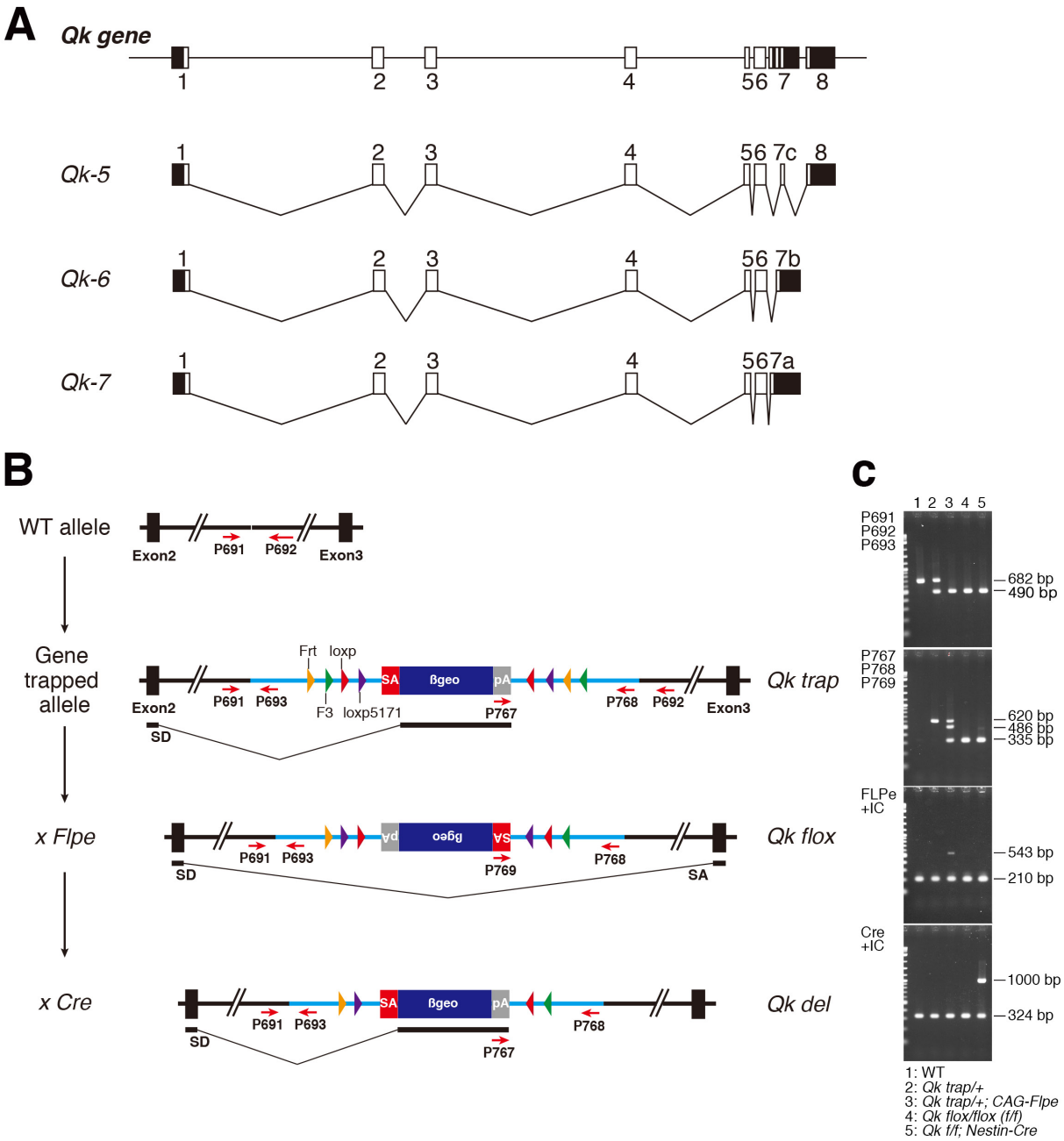

Figure S1. Scheme for the conditional targeting of *Qk* in mice; relating to Figures 2, 3, and 4

(A) A scheme showing the structure of *Qk* and its major alternative splice variants.

(B) Scheme for generating *Qk* conditional KO mice. A diagram of the targeted allele is

shown. *rsFlipROSAβgeo** was inserted into intron 2 of the *Qk* gene. Red arrows indicate the positions of primers for genotyping PCR. The "× *FLPe*" and "× *Cre*" diagrams show the inversion induced by Flippase and Cre recombinase by crossing with *FLPe* and *Cre* mice, respectively. The *Qk* gene is trapped and replaced by *βgeo* after exon2 by Cre-mediated inversion.

(C) Genotype PCR for distinguishing between wild-type allele (WT), gene trapped allele (*Qk trap*), floxed alleles (*Qk flox*) after FRT inversion; and KO alleles (*Qk del*) after Cre inversion. Primer pairs used for each genotyping PCR are indicated in **(B)** (refer to Transparent Methods subsection Mice). *FLPe* and *Cre* transgenes were detected using an internal control (IC).

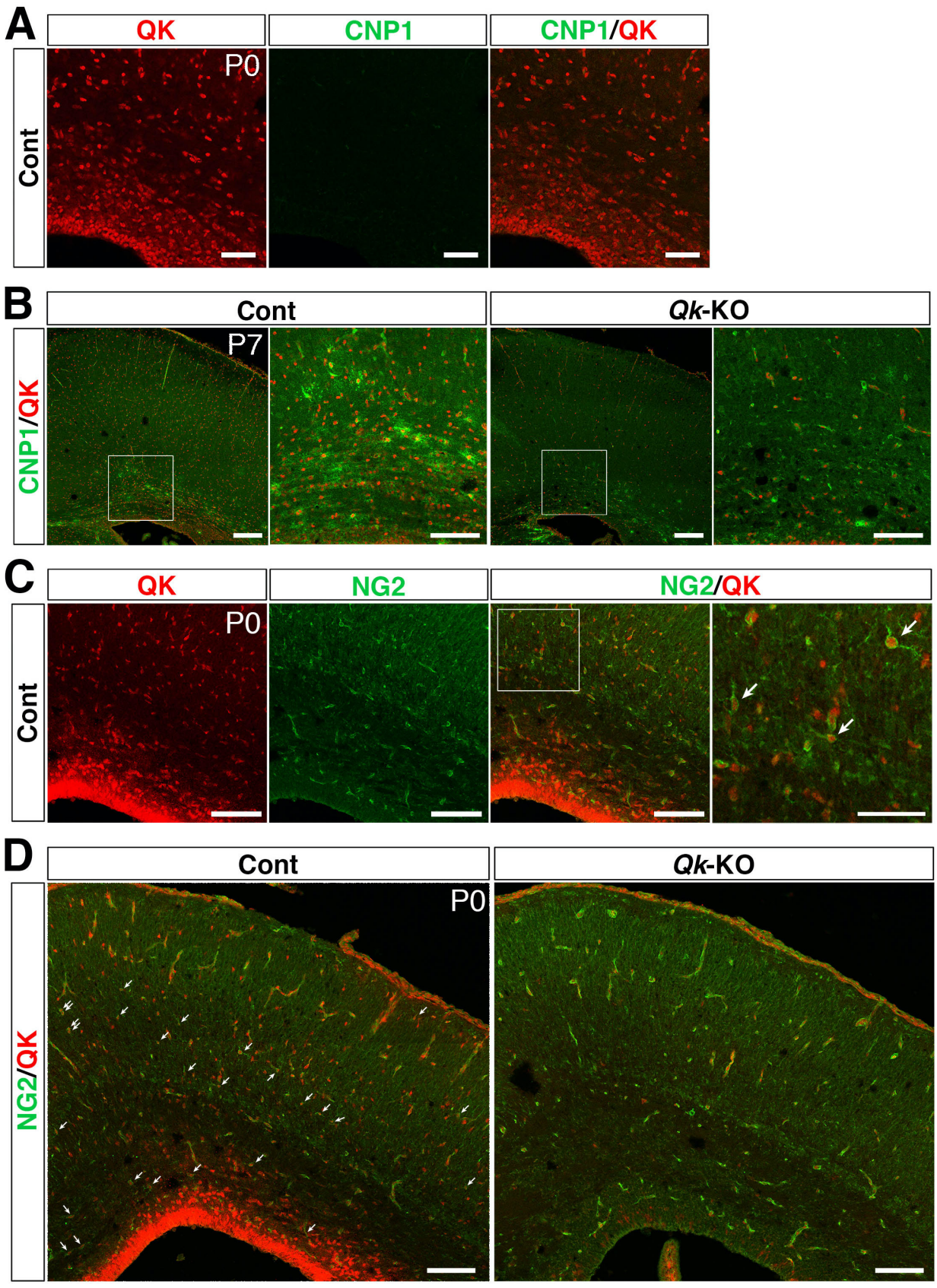
A
QK
CNP1
CNP1/QK
Cont
P0
B
Cont
Qk-KO
CNP1/QK
P7
C
QK
NG2
NG2/QK
Cont
P0
D
Cont
Qk-KO
NG2/QK
P0

Figure S2. NG2^{+} cells express QK and loss of *Qk* abolishes NG2 cells; relating to Figures 2, 3, and 4

(A) Co-Immunostaining of QK (red) and CNP1 (green) in the coronal sections of P0 control (Cont) cortex. Scale bar = 50 μm. **(B)** Co-Immunostaining of QK (red) and CNP1 (green) in the coronal sections of P7 Cont and *Qk*-KO cortices. The boxed areas in the 1st (Cont) and the 3rd (*Qk*-KO) panels from the left are shown at higher magnification in the 2nd and the 4th panels, respectively. Scale bar = 100 μm (the 1st and the 3rd panels) and 50 μm (the 2nd and the 4th panels). **(C)** Co-Immunostaining of QK (red) and NG2 (green) in the coronal sections of P0 Cont cortex (left three panels). The boxed area in the NG2/QK panel is shown at higher magnification in the right-most panel. Arrows indicate NG2-positive polydendrocytes (non-vascular cells), designated as NG2 cells showing highly branched morphology distinguished as the oligodendrocyte lineage cells. Scale bar = 100 μm in left three panels and 50 μm in the right-most panel. **(D)** Co-Immunostaining of QK (red) and NG2 (green) in the coronal sections of P0 Cont and *Qk*-KO cortices. Arrows indicate NG2-positive polydendrocytes cells, not be detected in *Qk*-KO cortex. Scale bar = 100 μm.

A Cell type-specific expression pattern of *Qk* in P0 Cerebal Cortex

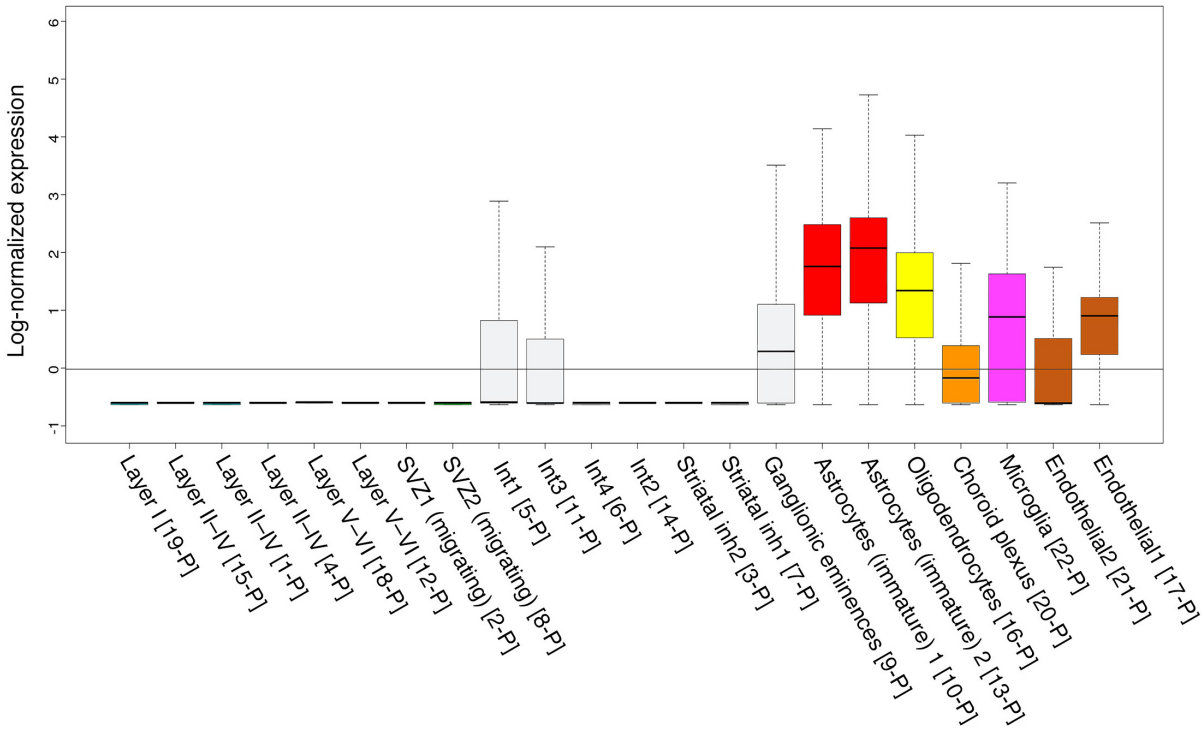

B Proportion of *Qk+* cells in P0 Cerebal Cortex

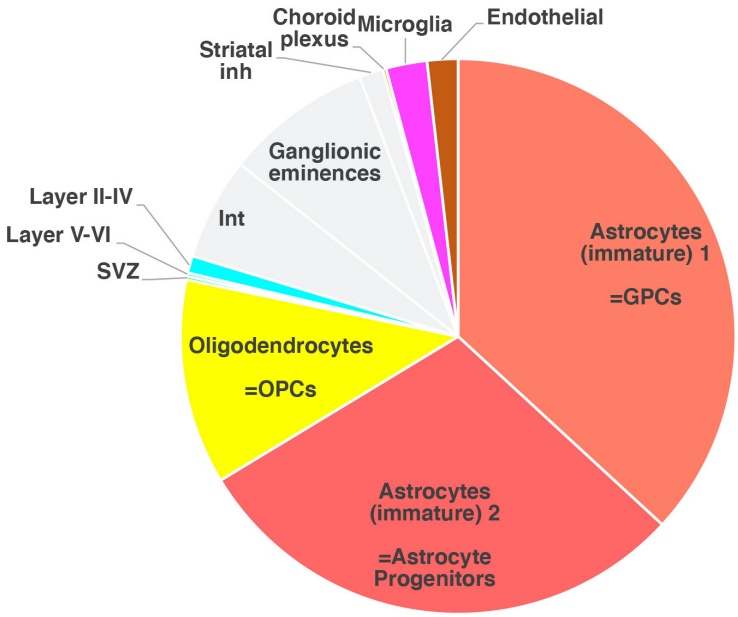

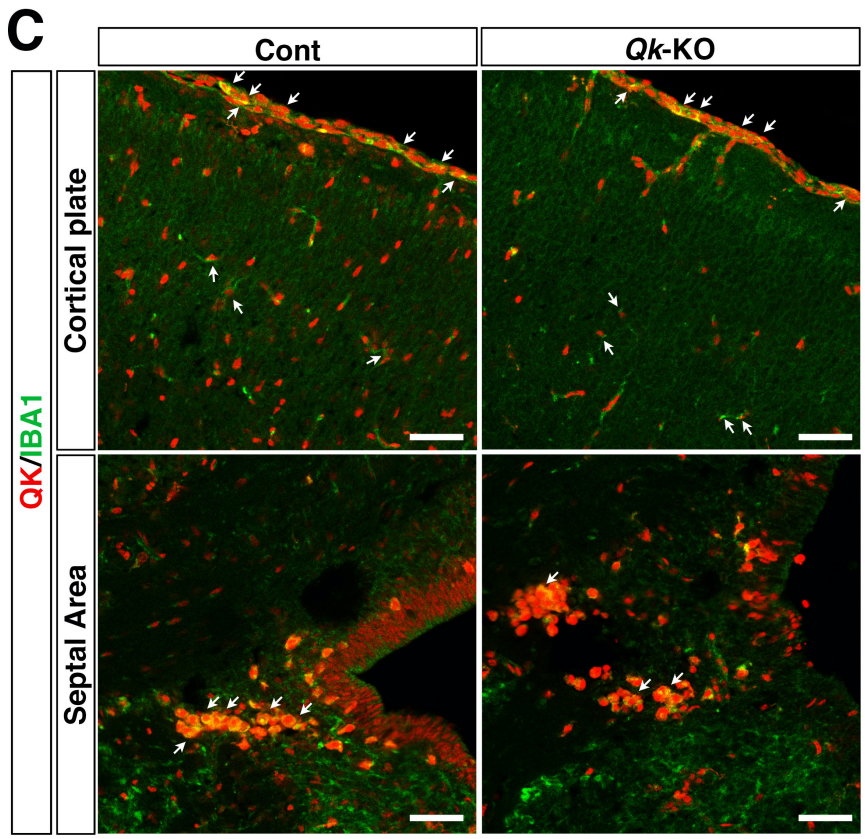
C
Cont
Qk-KO
QK/IBA1
Cortical plate
Septal Area

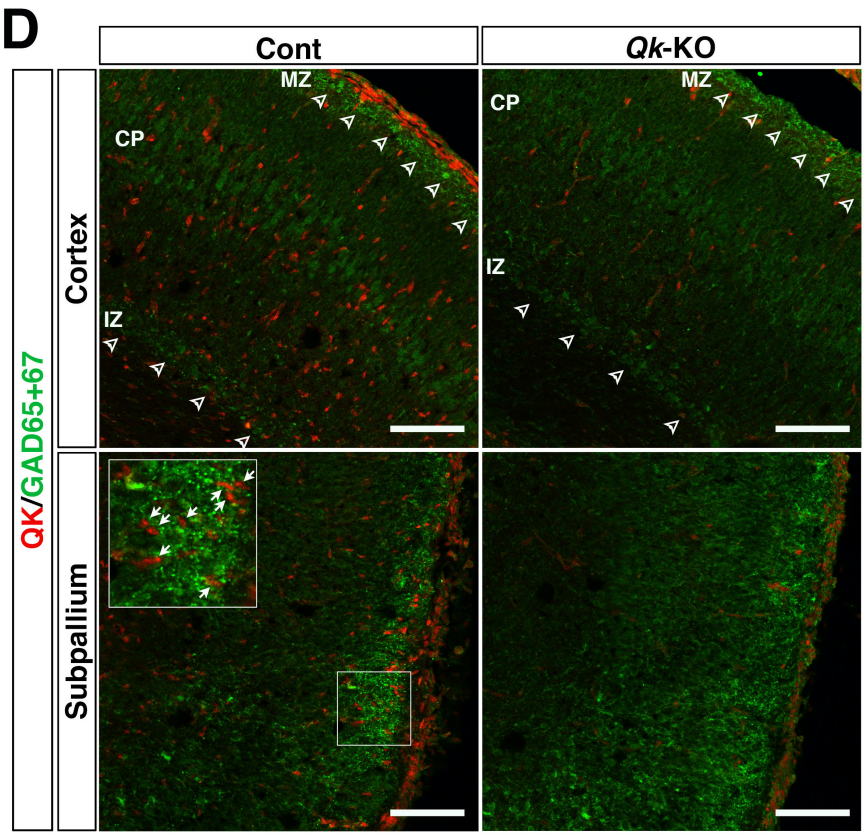
D
Cont
Qk-KO
QK/GAD65+67
Cortex
Subpallium
MZ
CP
IZ

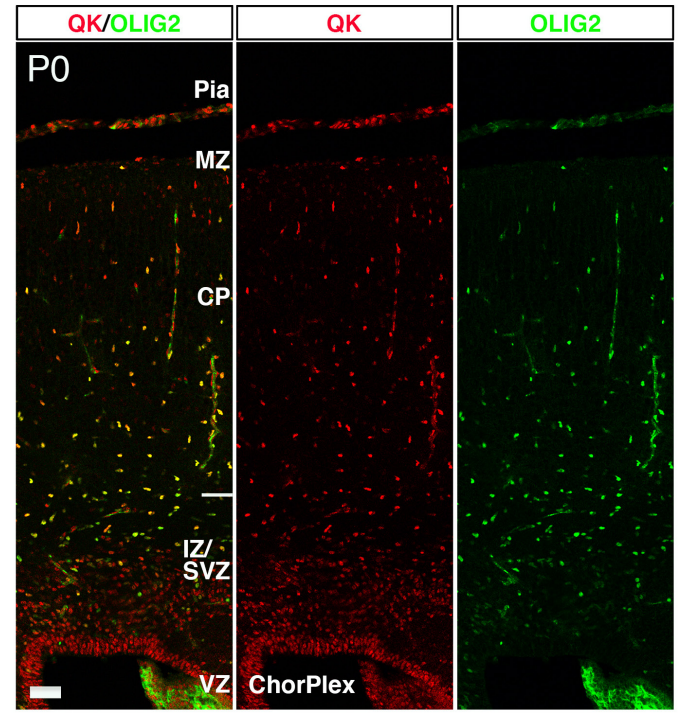

QK+ cells in P0 Cerebral Cortex	
Pia mater (containing microglia) (QK+, IBA1+)	3.0 %
Endothlial + Others (containing microglia)	6.3 %
Glial Progenitors (QK+, OLIG2+) = Astrocyte Progenitors and OPCs, containing NG2 cells (0.48 % of total)	23.2 %
GPCs in SVZ (QK+, OLIG2-, PDGFRα-) containing NG2 cells (0.19 % of total)	45.6 %
NSCs in VZ (QK+, NES+)	21.9 %
Choroid Plexus (not counted)	-
total	100 %

Figure S3. Qk is expressed in microglial cells in the pia mater and interneurons in the subpallium, in P0 brains; relating to Figures 1, 2, 3, and 4

(A) Identification of *Qk*-expressing cells in P0 cortices using single-cell transcriptomic analysis data of developing mouse neocortices (http://zylkalab.org/data). The cell population classified as Astrocytes (immature) 1, expressing both radial glial cell and astrocyte markers but lacking *Olig2* expression, can be considered as GPCs. Astrocytes (immature) 2, expressing the marker of Astrocyte-restricted precursor cells and also *Olig2*, can be considered as astrocytes progenitors. Non-neocortical cells in the

ganglionic eminences, the striatal inhibitory neurons, and the thalamus are included from adjacent non-cortical tissues.

(B) Proportion of *Qk*-expressing cells (Z-score ≥ 2) in E14 and P0 cortices. Non-cortical cells are also included from non-cortical tissues; shown with bright gray color.

(C) Co-Immunostaining of QK (red) and IBA1 (green) in the coronal sections of P0 control (Cont) and *Qk*-KO cortices. Arrows indicate double-positive cells. QK is expressed in IBAI-positive microglial cells in the pia mater and in the septal area. A smaller number of ramified shaped microglial cells, which were weakly positive for IBAI (compared with the pia mater staining) and positive for QK, was observed in the cortical plate (arrows in the Cortical Plate). Scale bar = 50 μm.

(D) Co-Immunostaining of QK (red) and GAD65/GAD67 (green) in the coronal sections of P0 Cont and *Qk*-KO cortices. Weak QK expression was detected in the subpallium where GAD65/GAD67-positive cells were accumulating (arrows), indicating QK expression in newly generated interneurons. However, tangentially migrating interneurons in the cerebral cortex were no longer positive for GAD65/GAD67 (open arrowhead), suggesting that QK expression in interneurons may be lost during differentiation, as we observed in cortical neurons (**Figure 1C**). Scale bar = 100 μm. Abbreviations are the same as in Figure 1A.

(E) Representative image of QK+ cells in the coronal sections of P0 Cont cortex co-immunostained with QK (red) and OLIG2 (green). The proportion of QK-positive cells is shown. Scale bar = 50 μm. Abbreviations: ChorPlex, Choroid plexus; the remaining are the same as in Figure 1A.

Glia-enriched genes		
Gene	Log2 FC	QRE in 3'UTR
Qk	-2.41	1
Gatm	-2.13	2
S100b	-1.69	1
Gng12	-1.53	6
Reep3	-1.15	6
Rab5a	-1.12	4
Abcd3	-1.12	1
Sept2	-1.06	4
Klhl5	-0.93	3
Degs1	-0.92	1
Gpm6b	-0.91	3
Scd1	-0.91	3
1810037I17Rik	-0.88	2
Cldnd1	-0.86	3
Vps35	-0.85	2
Abhd4	-0.81	1
Spag9	-0.79	5
Hdhd2	-0.78	2
Tmem9b	-0.67	1
Dmwd	-0.65	2
Srp14	-0.64	1
Pea15a	-0.63	3
Ankrd40	-0.62	4
Pcnp	-0.60	3
Canx	-0.60	2
Gmfb	-0.59	1
Tmem30a	-0.59	3

Astrocyte-enriched genes		
Gene	Log2 FC	QRE in 3'UTR
Vcam1	-2.36	1
Luzp2	-1.76	5
Slc1a3	-1.43	3
Sfxn5	-1.33	2
Ednrb	-1.13	2
Abhd3	-1.07	1
Ptprz1	-0.97	2
Gja1	-0.87	2
Axl	-0.81	1
Mfap3l	-0.80	7
Ddah1	-0.79	4
Spag9	-0.79	5
Aldh6a1	-0.75	4
Slc4a4	-0.71	4
Tril	-0.69	1
Tiparp	-0.66	3
Gria2	-0.65	7

OL-enriched genes		
Gene	Log2 FC	QRE in 3'UTR
Qk	-2.41	1
Gatm	-2.13	2
S100b	-1.69	1
Gng12	-1.53	6
Il1rap	-1.42	4
Ugt8a	-1.28	4
Prkcq	-1.23	1
Reep3	-1.15	6
Abcd3	-1.12	1
Sept2	-1.06	4
Klhl5	-0.93	3
Degs1	-0.92	1
Gpm6b	-0.91	3
Scd1	-0.91	3
1810037I17R	-0.88	2
Cldnd1	-0.86	3
Vps35	-0.85	2
Gpr155	-0.84	1
Plekhb1	-0.83	1
Abhd4	-0.81	1
Hdhd2	-0.78	2
Tmem9b	-0.67	1
Omg	-0.67	1
Sbds	-0.66	1
Dmwd	-0.65	2
Srp14	-0.64	1
Pea15a	-0.63	3
Ankrd40	-0.62	4
Pcnp	-0.60	3
Canx	-0.60	2
Gmfb	-0.59	1
Tmem30a	-0.59	3

OPC-enriched genes		
Gene	Log2 FC	QRE in 3'UTR
Luzp2	-1.76	5
Cav2	-1.68	2
Pcdh15	-1.46	4
Il1rap	-1.42	4
Pdgfra	-1.26	1
Prkcq	-1.23	1
Ednrb	-1.13	2
Tmem100	-1.12	1
Ccnd1	-1.05	1
Ampd3	-1.03	2
Ptprz1	-0.97	2
Cadm2	-0.95	4
Spon1	-0.94	5
Gpm6b	-0.91	3
Fchsd2	-0.90	1
Chpt1	-0.89	2
Spred1	-0.87	8
Gpr155	-0.84	1
Galc	-0.84	3
Timp4	-0.82	1
Ddah1	-0.79	4
Fubp3	-0.76	1
Tspan12	-0.74	3
Cx3cl1	-0.72	1
Lhfpl3	-0.70	7
Snx27	-0.70	6
Omg	-0.67	1
Gria2	-0.65	7
Taf9b	-0.64	1
Ipo5	-0.64	2
Farp1	-0.64	1
Nckap1	-0.63	1

Neuron-enriched genes		
Gene	Log2 FC	QRE in 3'UTR
Wnt7b	-1.34	1
Cx3cl1	-0.72	1

Supplementary Table S1. Downregulated genes with QRE in *Qk*-KO NSCs induced glial differentiation, relating to Figure 5, 6

Experimental Procedures (continued)

Mice

Conditional KO mice for *Qk* were generated using the gene-trapped ES (embryonic stem) cell line EUCE0299b07 (Schnutgen et al., 2005) obtained from the European Conditional Mouse Mutagenesis Program. The gene structure of *Qk* and the targeting scheme is shown in **Figure S1A** and **S1B**. In this cell line, the *Qk* gene is trapped after exon 2, resulting in the deletion of > 85.2% of the coding region (in the case of *Qk-6*) beginning from the middle portion of the QUA1 domain at the N-terminus. The generation of chimeric mice is described elsewhere (Takeuchi et al., 2018); these mice were crossed with *CAG-FLPe* mice (RIKEN BioResource Center, Tsukuba, Japan) (Kanki et al., 2006) to inactivate gene trapping and create a floxed allele by FRT (Flp recombination target)-induced inversion. These mice were further crossed with a *Nestin-Cre* (Tronche et al., 1999) line to induce NSC-specific KO mice. Genotyping PCR was performed using genomic DNA from the tail or yolk sac. Embryonic stages were calculated using noon (12:00 PM) of the vaginal plug day as the reference time point E0.5. The scheme for gene trapping, FRT-induced inversion, Cre-induced gene trapping, and genotyping primer positions with the results of genotyping PCR are shown in **Figure S1B** and **S1C**. See manuscript for the detailed gene targeting

strategy (Schnutgen et al., 2005). Genotyping PCR was carried out to distinguish between the wild-type (WT) allele, gene-trapped allele (*Qk trap*), and floxed allele (*Qk floxed*) after FRT-induced inversion; and Cre-induced gene trapping (*Qk del*) for *Qk*. *FLPe* and *Cre* transgenes were detected by PCR with the internal control (IC) (IC: *Tcrd* for *FLPe* and *IL-2* for *Cre*) (**Figure S1C**). Mice of *wt, wt;Nestin-Cre,* $Qk^{f/f}$*, and* $Qk^{f/+}$, litter mates of heterozygous and homozygous mutant mice, were used as controls. All animal care and experiments were conducted in accordance with the U.S. National Institutes of Health Guide for the Care and Use of Laboratory Animals, and all experimental protocols were approved by the Institutional Animal Care and Use Committee of the Kyoto University Graduate School of Medicine and the RIKEN Kobe Branch.

Primers for detection of WT, *trap*, and *f* alleles and *del*

P691	5′- GTGCTGCATTCAGTTACTACATCC-3′
P692	5′- CATCACCATCGCCAGTTCTCGTCC-3′
P693	5′- GTCCTCCGATTGACTGAGTCGC-3′
P767	5′- ATCAGCCTCGACTGTGCCTTCTAG -3′
P768	5′- TCCAGCCCTCACTCCTTCTCTAG-3′
P769	5′- CAAGGAAACCCTGGACTACTGCG-3′

Primers for detection of *CAG-FLPe* with internal control

P0087-2	5′-GCTCTAGAGCCTCTGCTAACCATGTTCATG-3′
P720	5′-TCCATGAGTGAACGAACCTGGTCGAAATCAG-3′
P715	5′-CTAGGCCACAGAATTGAAAGATCT-3′
P716	5′-GTAGGTGGAAATTCTAGCATCATCC-3′

Primers for detection of *Nestin-Cre* with internal control

P719	5′-GAAGCCGAGTCTCAGAGAATTTGAGTGTG-3′
P720	5′-TCCATGAGTGAACGAACCTGGTCGAAATCAG-3′
P715	5′-CTAGGCCACAGAATTGAAAGATCT-3′
P716	5′-GTAGGTGGAAATTCTAGCATCATCC-3′

DNA Constructs

3'UTR QRE reporter constructs

To construct 3'UTR QRE reporter vectors, the 3'UTR sequences of *Rab5a*, *Snx5*, *Cbl*, and *Cav1* genes were isolated from C57BL/6 genomic DNA and ligated into the 3'-end of *eGFP* cDNA in pcDNA3.1(+) at the *XhoI/EcoRI* or *XhoI/BamHI* sites. Vectors in which QRE in the 3'UTR were mutated from ACTAAH (H = not G) to TCGAGH were generated by Gene Synthesis (Eurofins Genomics, Ebersberg, Germany). The following primers were used for amplification of the 3'UTR sequences:

Rab5a-F (P1131)	5′-CAC CCT CGA GAC CAC CAG GTT GTT TTC TGT TTG AG-3′
Rab5a-R (P1132)	5′-TTG GAT CCA GCC TTT ATA CAA GTC CGT TT-3′
Snx5-F (P1163)	5′-CAC CCT CGA GCC TGT CTA CTC TGA AGG ACA CC-3′
Snx5-R (P1164)	5′-TTG AAT TCG TTG TGA AAT CTT TTC TTA AAT AAA TC-3′
Cbl-F (P1157)	5′-CAC CCT CGA GCA CAT CTC TCC CTG CCA CGG CTT C-3′
Cbl-R (P1158)	5′-TTG GAT CCA TGT ATT TAT TTA ATG CTC TAC CTG-3′
Cav1-F (P1169)	5′-CAC CCT CGA GGG GAC ATT TCA AGG ATG AAA GG-3′
Cav1-R (P1170)	5′-TTG GAT CCG CGT AAC TGT TAA ACA ATT TTA TTG TG-3′

***Qk* expression vectors**

The full-length mouse *Qk-7* coding sequence (NM_021881.2) was isolated from P7 mouse brain cDNA and cloned into the pENTR D-Topo vector (Thermo Fisher Scientific, Waltham, MA, USA). To construct the *Qk-6* expression vector, a PCR-based modification was introduced into the C-terminus of *Qk-7* cDNA to generate the full-length *Qk-6* coding sequence (NM_001159516.1) and the fragment was cloned into the pCAG-3×FLAG-DEST vector. To generate a *Qk-6* expression vector with QUA1 deletion (Qk-6 ΔQUA1) (Chen and Richard, 1998; Ryder and Massi, 2010), a PCR-based deletion was introduced into the N-terminal domain of the full-length *Qk-6* coding

sequence and the fragment was cloned into the pcDNA5_FRT-TO-3×FLAG-DEST vector.

Primary neural stem/precursor cell (NS/PC) culture and differentiation into astrocytes

NS/PCs were isolated from E14 mouse embryo (male and female) cortices. The tissue samples were triturated in Hank's balanced salt solution (Sigma-Aldrich, St. Louis, MO, USA; H2387). Dissociated cells were cultured for 4 days prior to experiments in N2 medium composed of Dulbecco's Modified Eagle's Medium (DMEM)/F12 (Gibco, Grand Island, NY, USA; 124000-24), 25 μg/ml insulin (Wako Pure Chemical Industries, Osaka, Japan; 097-06474), 100 μg/ml apo-transferrin (Nacalai Tesque, Kyoto, Japan; 34401-55), 16 μg/ml putrescine dihydrochloride (Sigma-Aldrich; P5780), 30 μM sodium selenite (Sigma-Aldrich; S5261), and 20 μM progesterone (Sigma-Aldrich; P0130) supplemented with 10 ng/ml bFGF (PeproTech, Rocky Hill, NJ, USA; 100-18B) on culture dishes coated with poly-L-ornithine (Sigma-Aldrich; P3655) and fibronectin (Sigma-Aldrich; F4759) at 37 °C and 5% CO_2. To induce glial differentiation, cells were seeded on dishes in N2 medium lacking bFGF but containing 10% fetal bovine serum (FBS).

Cell culture, transfection of Qk cDNA and 3'UTR reporter constructs, and quantitative (q)PCR

HeLa cells were cultured in DMEM containing 10% FBS, glutamine, and penicillin/streptomycin at 37 °C and 5% CO_2. The cells were transfected with the 3'UTR reporter constructs and Qk cDNA using Lipofectamine 2000 (Life Technologies, Carlsbad, CA, USA) according to the manufacturer's instructions, followed by incubation for 48 h. Total RNA was extracted from the cells and used to synthesize cDNA as previously described (Takeuchi et al., 2010); qPCR was performed using FastStart Universal SYBR Green Master (Rox) (Roche Diagnostics, Basel, Switzerland) on a StepOnePlus Real-Time PCR System (Applied Biosystems, Foster City, CA, USA). For the comparison of mRNA expression from different reporter vectors, each vector was co-transfected with Qk-6 lacking the QUA1 domain (Qk ΔQUA1), whose RNA binding activity is abolished (Chen and Richard, 1998; Ryder and Massi, 2010). mRNA levels were used as a negative control for Qk induction, as well as for normalization. Transfection efficiency was monitored using the SV40-Neo gene in the vector as an IC.

The PCR primer pairs used for qPCR were as follows:

FLAG-eGFP-F (P1133)	5′-ATG GAC TAC AAG GAC GAC GAT GAC-3′
FLAG-eGFP-R (P0088)	5′-ACG TCG CCG TCC AGC TCG AC-3′
Neomycin-F (P1184)	5′-GAT CTC CTG TCA TCT CAC CTT GC-3′
Neomycin-R (P1185)	5′-CTT GGT GGT CGA ATG GGC AGG TAG-3′

BrdU labeling and immunohistochemistry

Brain tissue sections were fixed with 4% paraformaldehyde in phosphate-buffered saline (PBS) (pH 7.4) for 15 min at room temperature, then subjected to heat-induced antigen retrieval in 10 mM citrate buffer (pH 6.0) using microwave 500V for 10 min. After permeabilization and blocking with blocking buffer at room temperature, the sections were incubated overnight at 4 °C, or for 2 h at room temperature, with primary antibodies, followed by secondary or tertiary antibodies for 2 h at room temperature. BrdU labeling was performed as previously described (Takeuchi et al., 2007). Briefly, pregnant mice were intraperitoneally injected with BrdU (40 mg/kg) and 1 h later embryos were collected, sectioned, and immunolabeled as described in a previous report (Tuttle et al., 1999). The primary antibodies were as follows: rat monoclonal anti-BrdU (1:100, cat. no. BU1/75[ICR1]; Novas Biologicals, Littleton, CO, USA); mouse anti-Acsbg1 (1:400, cat. no. ab118154), and rabbit anti-CNP1 (1:200, cat. no. ab6319) (all from Abcam, Cambridge,

UK); mouse anti-GFAP (1:400, cat. no. G 3893; Sigma-Aldrich); rabbit anti-QK (1:200, cat. no. IHC-00574; Bethyl Laboratories, Montgomery, TX, USA); mouse monoclonal anti-Tuj1 (1:500, cat. no. MMS-435P) and mouse anti-MBP (1:800, cat. no. SMI-99P) (from Covance, Princeton, NJ, USA); rabbit anti-PDGFRα (1:1000; cat. no. sc-338, Santa Cruz Biotechnology, Santa Cruz, CA, USA); and mouse anti-QK (1:200, cat. no. MABN624), rabbit anti-SOX2 (1:800, cat. no. AB5603), mouse anti-OLIG2 (1:1000, cat. no. MABN50), and rabbit anti-NG2 (1:200, cat. no. AB5320) (all from Merck, Darmstadt, Germany). The secondary antibodies were as follows: goat anti-rabbit Alexa Fluor 488 (1:200, cat. no. A-11070), goat anti-rabbit Alexa Fluor 555 (1:200, cat. no. A-21430), donkey anti-rat Alexa Fluor 488 (1:200, cat. no. A-21208), donkey anti-mouse Alexa Fluor 647 (1:200, cat. no. A-31571), goat anti-mouse Alexa Fluor 488 (1:200, cat. no. A-11001), and Alexa Fluor 488 and Alexa Fluor 555 streptavidin conjugate (both 1:200, cat. nos. S11223 and S32355) (all from Thermo Fisher Scientific); and biotinylated goat anti-rabbit IgG (1:100, cat. no. BA-1000; Vector Laboratories, Burlingame, CA, USA). Nissl staining was performed according to standard procedures with 0.1% cresyl violet solution. Sections were incubated with Hoechst 33258 (1:500, cat. no. 04928-92; Nacalai Tesque) for nuclear staining and mounted using ProLong Gold Antifade Reagent (Thermo Fisher Scientific). Fluorescence images were acquired on a DM6000 digital microscope system or TCS SP8

confocal laser scanning microscopy (Leica, Wetzlar, Germany). For quantification, all digital images were processed using ImageJ software (https://imagej.nih.gov/ij/docs/index.html). We counted PDGF-Rα$^+$, OLIG2$^+$, ACSBG1$^+$, and GFAP$^+$ cells in the dorsal to the lateral palliums of the frontal cerebrums: cortical strips 500 μm wide for P0 and 1000 μm for P7 from the frontal cortices per each brain.

Immunocytochemistry

Cells were fixed at the indicated days *in vitro* (DIV) with 4% paraformaldehyde in PBS, permeabilized and blocked with blocking buffer (3% FBS and 0.1% Triton X-100 in PBS). The cells were probed with the following antibodies: rabbit anti-SOX2 (1:400) and mouse anti-ACSBG1 (1:400), followed by goat anti-rabbit Alexa Fluor 488 (1:800, cat. no. A-11008; Thermo Fisher Scientific) and goat anti-mouse Alexa Fluor 555 (1:800). Sections were incubated with Hoechst 33342 (1:500) for nuclear staining and mounted using ProLong Gold Antifade Reagent. Fluorescence images were acquired using a DM6000 digital microscope system or TCS SP8 confocal laser scanning microscopy (Leica, Wetzlar, Germany). For quantification, all digital images were processed using ImageJ software (https://imagej.nih.gov/ij/docs/index.html).

Western blotting

Cerebral cortices were isolated from Cont and *Qk-KO* embryos, proteins were extracted using sample buffer (Nacalai Tesque, Kyoto, Japan), and the lysates were denatured at 95 °C for 3 min and sonicated. Protein concentrations were quantified with Pierce 660nm Protein Assay Reagent and Ionic Detergent Compatibility Reagent for Pierce 660nm Protein Assay Reagent (Thermo Fisher Scientific). They were then resolved by SDS-PAGE (SuperSep Ace gel; Wako Pure Chemical Industries) and transferred to a polyvinylidene difluoride membrane (Pall Corporation, Port Washington, NY, USA). Antibody reactions were performed with Can Get Signal immunoreaction enhancer solution (Toyobo, Osaka, Japan). Immunoreactivity was visualized with Chemi-Lumi One Super (Nacalai Tesque) or ImmunoStar LD (Wako Pure Chemical Industries) and a ChemiDoc MP imaging system (Bio-Rad, Hercules, CA, USA). The following primary antibodies were used in this study: rabbit anti-QK (1:4000), mouse anti-GFAP (1:20000), mouse monoclonal anti-ACSBG1 (1:4000), mouse monoclonal anti-OLIG2 (1:2000), rabbit anti-PDGF-Rα (1:2000), and mouse monoclonal αTUBULIN (1:1000 or 1:5000, cat. no. #2125, Cell Signaling Technology, Danvers, MA, USA). Horseradish peroxidase-conjugated anti-rabbit IgG (cat. no. NA934) and anti-mouse IgG (cat. no. ab5887) were from GE Healthcare Life Sciences (Pittsburgh, PA, USA) and Abcam, respectively.

Exon Array analysis of NSC- and neuron-specific layers

Cranial regions were isolated from E15.5 C57BL/6 mouse embryos, embedded in OCT (optimal cutting temperature) compound (Sakura Finetechnical Co., Tokyo, Japan), frozen, and sectioned at a thickness of 20 μm on a cryostat (CM-3050; Leica). The sections were collected on MembraneSlides (PEN membrane 2.0 μm; Leica) and stained with Arcture HistoGene Staining Solution (Thermo Fisher Scientific) under RNase-free conditions according to the manufacturer's instructions. The lower and upper areas of the entire cortex (harboring NSC- and neuron-specific regions, respectively) from rostral to caudal were isolated using a laser capture microdissection system (LMD6; Leica) (scheme in **Figure 1A**). Total RNA was isolated from three separate brains (n = 3 each for upper and lower regions) using the RNeasy Micro kit (Qiagen) and subjected to Exon Array analysis. The quality of extracted RNA was evaluated with an Agilent RNA 6000 Nano and BioAnalyzer; the RNA integrity number (RIN) was 8.60–9.40. cDNA labeling, hybridization, and signal acquisition of the GeneChip Mouse Exon 1.0 ST Exon Array (Affymetrix, Santa Clara, CA, USA) were performed as previously described (Ishigaki et al., 2012).

Bioinformatics analysis of exon array data

Bioinformatics analysis of exon array data was performed as previously described (Yamashita et al., 2012). Visualization and cluster analysis of expression values were performed with MultiExperiment Viewer (Saeed et al., 2006) using the probe set information provided by Affymetrix. Data were normalized with the Sketch-Quantile method implemented in Affymetrix Expression Console software.

Comparative analysis of RNA-seq data

RNA profiles were then determined from mRNA-seq data (from polyA-selected mRNA). mRNA-seq reads were subjected to quality control; reads from rRNA/tRNA or repetitive regions (Bao et al., 2015), average quality scores < 17, and length < 50 nt were filtered out. Those that passed the quality control were mapped to the Mus musculus genome (mm10) with the STAR aligner (v.2.4.1d) (Dobin et al., 2013). The genome sequence was indexed with splicing junction information from Ensembl v.83. For quantification of gene expression levels, we calculated transcripts per millions (TPM) values for each locus using RSEM (v.1.3.0). We initially calculated read per kilobase 10 million (RPK10M) for each gene and scaled these values into TPM values. A gene was defined as expressed when the TPM value was ≥ 2. For differential gene expression analysis, we used DEseq2 (Love et

al., 2014). Genes that met the following criteria were considered as differentially expressed: Log2 FC > 0.58 (FC > 1.5) or Log2 FC < −0.58 (FC < 0.67); an adjusted *p*-value < 0.01; raw tag count ≥ 31 for at least one condition (Cont or *Qk-KO*); and TPM ≥ 2 for at least one condition for primary cells. To evaluate the change in gene expression, we generated cell-type enriched gene lists for astrocytes, OLs, OPCs, glia (astrocytes + OPCs + OLs), or neurons referring the neural and glial cell type-specific transcriptome databases of the mouse cerebral cortex (Zhang et al., 2014): the 500 most enriched genes in the indicated cell types were listed. The raw data from mRNA-seq were deposited in the Gene Expression Omnibus (GEO) under accession number GSE117018.

Analysis of Single-cell transcriptomic data from developing mouse neocortex.

To detect in a full extent *Qk*-expressing cells, we re-analyzed data from single-cell RNA-seq (scRNA-seq) obtained by the Zylka's group in the context of mouse P0 cerebral cortex (Loo et al., 2019) (NCBI GEO accession No; GSE12333). To draw boxplots representing the gene expression values in each cell types, raw read counts were converted into log-normalized expression values using the published scripts2 (https://github.com/jeremymsimon/MouseCortex). The cell types were defined as per the original annotation (Loo et al., 2019). To draw the pie-chart referent to *Qk*-expressing cells'

distribution, only cells showing *Qk* log-normalized expression values ≥ 2.0 were considered as *Qk*-positive cells.

Data and code availability

All data are available from the GEO under the accession number GSE117018. In-house scripts were used to calculate RPKM and TPM. All data and scripts not included here are available from the corresponding author upon reasonable request.

GSEA

Expressed genes (TPM ≥ 2.0, see "Comparative analysis of RNA-seq data from brains and NSCs" in METHODS) served as the input for GSEA (http://software.broadinstitute.org/gsea/index.jsp) (Subramanian et al., 2005), using GSEA v3.0 with default parameters (except for permutation type, which was changed to "gene set"). Cell type-specific gene lists were used for analysis (see "Comparative analysis of RNA-seq data from NSCs " in the Supplemental Material and Methods section).

Gene Ontology

Gene Ontology analysis was performed using the DAVID (Database for Annotation,

Visualization, and Integrated Discovery) Bioinformatics Resources (http://david.niaid.nih.gov). For background genes, we used all expressed genes from our RNA-seq data (see "Comparative analysis of RNA-seq data from brains and NSCs" in the Supplemental Material and Methods section).

Statistics

Values are presented as mean ± SD or SEM. Statistical analyses were performed by two-tailed Student's or Welch's *t*-test using JMP software. Probabilities of $p < 0.05$ were considered significant. Statistical analysis of RNA-seq was evaluated with DEseq2 to analyze differentially expressed genes (http://www.bioconductor.org/packages/release/bioc/html/DESeq2.html.) (Love et al., 2014). Statistical analysis of GSEA data was evaluated with GSEA 2.0 (http://software.broadinstitute.org/gsea/index.jsp) (Subramanian et al., 2005) with default parameters (except for the permutation type, which was changed to "gene set").

Supplemental References

Bao, W., Kojima, K.K., and Kohany, O. (2015). Repbase Update, a database of repetitive elements in eukaryotic genomes. Mob DNA *6*, 11.

Chen, T., and Richard, S. (1998). Structure-function analysis of Qk1: a lethal point mutation in mouse quaking prevents homodimerization. Mol. Cell. Biol. *18*, 4863-4871.

Dobin, A., Davis, C.A., Schlesinger, F., Drenkow, J., Zaleski, C., Jha, S., Batut, P., Chaisson, M., and Gingeras, T.R. (2013). STAR: ultrafast universal RNA-seq aligner. Bioinformatics *29*, 15-21.

Ishigaki, S., Masuda, A., Fujioka, Y., Iguchi, Y., Katsuno, M., Shibata, A., Urano, F., Sobue, G., and Ohno, K. (2012). Position-dependent FUS-RNA interactions regulate alternative splicing events and transcriptions. Sci. Rep. *2*, 529.

Kanki, H., Suzuki, H., and Itohara, S. (2006). High-efficiency CAG-FLPe deleter mice in C57BL/6J background. Exp. Anim. *55*, 137-141.

Loo, L., Simon, J.M., Xing, L., McCoy, E.S., Niehaus, J.K., Guo, J., Anton, E.S., and Zylka, M.J. (2019). Single-cell transcriptomic analysis of mouse neocortical development. Nat Commun *10*, 134.

Love, M.I., Huber, W., and Anders, S. (2014). Moderated estimation of fold change and dispersion for RNA-seq data with DESeq2. Genome Biol. *15*, 550.

Ryder, S.P., and Massi, F. (2010). Insights into the structural basis of RNA recognition by STAR domain proteins. Adv. Exp. Med. Biol. *693*, 37-53.

Saeed, A.I., Bhagabati, N.K., Braisted, J.C., Liang, W., Sharov, V., Howe, E.A., Li, J., Thiagarajan, M., White, J.A., and Quackenbush, J. (2006). TM4 microarray software suite. Methods Enzymol. *411*, 134-193.

Schnutgen, F., De-Zolt, S., Van Sloun, P., Hollatz, M., Floss, T., Hansen, J., Altschmied, J., Seisenberger, C., Ghyselinck, N.B., Ruiz, P.*, et al.* (2005). Genomewide production of multipurpose alleles for the functional analysis of the mouse genome. Proc. Natl. Acad. Sci. U. S. A. *102*, 7221-7226.

Subramanian, A., Tamayo, P., Mootha, V.K., Mukherjee, S., Ebert, B.L., Gillette, M.A., Paulovich, A., Pomeroy, S.L., Golub, T.R., Lander, E.S.*, et al.* (2005). Gene set enrichment analysis: a knowledge-based approach for interpreting genome-wide expression profiles. Proc. Natl. Acad. Sci. U. S. A. *102*, 15545-15550.

Takeuchi, A., Hamasaki, T., Litwack, E.D., and O'Leary, D.D. (2007). Novel IgCAM, MDGA1, expressed in unique cortical area- and layer-specific patterns and transiently by distinct forebrain populations of Cajal-Retzius neurons. Cereb. Cortex *17*, 1531-1541.

Takeuchi, A., Hosokawa, M., Nojima, T., and Hagiwara, M. (2010). Splicing reporter mice revealed the evolutionally conserved switching mechanism of tissue-specific alternative exon selection. PLoS One *5*, e10946.

Takeuchi, A., Iida, K., Tsubota, T., Hosokawa, M., Denawa, M., Brown, J.B., Ninomiya, K., Ito, M., Kimura, H., Abe, T.*, et al.* (2018). Loss of Sfpq Causes Long-Gene Transcriptopathy in the Brain. Cell Rep. *23*, 1326-1341.

Tronche, F., Kellendonk, C., Kretz, O., Gass, P., Anlag, K., Orban, P.C., Bock, R., Klein, R., and Schutz, G. (1999). Disruption of the glucocorticoid receptor gene in the nervous system results in reduced anxiety. Nat. Genet. *23*, 99-103.

Tuttle, R., Nakagawa, Y., Johnson, J.E., and O'Leary, D.D. (1999). Defects in thalamocortical axon pathfinding correlate with altered cell domains in Mash-1-deficient mice. Development *126*, 1903-1916.

Yamashita, Y., Matsuura, T., Shinmi, J., Amakusa, Y., Masuda, A., Ito, M., Kinoshita, M., Furuya, H., Abe, K.,

Ibi, T., *et al.* (2012). Four parameters increase the sensitivity and specificity of the exon array analysis and disclose 25 novel aberrantly spliced exons in myotonic dystrophy. J. Hum. Genet. *57*, 368-374.
Zhang, Y., Chen, K., Sloan, S.A., Bennett, M.L., Scholze, A.R., O'Keeffe, S., Phatnani, H.P., Guarnieri, P., Caneda, C., Ruderisch, N., *et al.* (2014). An RNA-sequencing transcriptome and splicing database of glia, neurons, and vascular cells of the cerebral cortex. J. Neurosci. *34*, 11929-11947.